RMetS
Royal Meteorological Society

The k^{-1} scaling of air temperature spectra in atmospheric surface layer flows

D. Li,[a]* G. G. Katul[b,c] and P. Gentine[d]
[a]*Program of Atmospheric and Oceanic Sciences, Princeton University, NJ, USA*
[b]*Nicholas School of the Environment, Duke University, Durham, NC, USA*
[c]*Department of Civil and Environmental Engineering, Duke University, Durham, NC, USA*
[d]*Department of Earth and Environmental Engineering, Columbia University, New York, NY, USA*

*Correspondence to: D. Li, Program of Atmospheric and Oceanic Sciences, 300 Forrestal Road, Sayre Hall, Princeton University, Princeton, NJ 08544, USA. E-mail: danl@princeton.edu

A number of atmospheric surface layer (ASL) experiments reported a k^{-1} scaling in air temperature spectra $E_{TT}(k)$ at low wavenumber k but other experiments did not. Occurrence of this scaling law in $E_{TT}(k)$ in an idealized ASL flow across a wide range of atmospheric stability regimes is investigated theoretically and experimentally using measurements collected above a lake and a grass surface. Experiments reveal a k^{-1} scaling persisted across different atmospheric stability parameter values (ζ) ranging from mildly unstable to mildly stable conditions ($-0.1 < \zeta < 0.2$). As instability increases, the k^{-1} scaling vanishes. Based on simplified spectral and co-spectral budgets and using a Heisenberg eddy viscosity as a closure to the spectral flux transfer term, conditions promoting a k^{-1} scaling in $E_{TT}(k)$ are identified. Existence of a k^{-1} scaling is shown to be primarily linked to an imbalance between the production and dissipation rates of half the temperature variance. When $-0.1 < \zeta < 0.2$, such imbalance exhibits weak dependence on ζ and hence z, which is shown to be the main cause for a -1 scaling at low k. As the atmosphere becomes more unstable, the imbalance determined from experiments here are not significantly affected by ζ, thereby negating conditions promoting a -1 scaling in $E_{TT}(k)$. The role of the imbalance between the production and dissipation rates of half the temperature variance in controlling the existence of a -1 scaling suggests that the -1 scaling in $E_{TT}(k)$ does not necessarily concur with the -1 scaling in the spectra of longitudinal velocity $E_{uu}(k)$. This finding explains why some ASL experiments reported k^{-1} in $E_{uu}(k)$ but not in $E_{TT}(k)$.

Key Words: atmospheric surface layer; co-spectral budget; Heisenberg's eddy viscosity; spectral budget; temperature spectra; k^{-1} scaling

Received 3 May 2015; Revised 3 August 2015; Accepted 10 September 2015; Published online in Wiley Online Library

1. Introduction

Since the Kansas experiments, the 'universal' or '$-5/3$' character of the Kolmogorov scaling in the inertial subrange of the velocity and air temperature spectra received much attention (Kaimal *et al.*, 1972; Wyngaard and Cote, 1972; Kaimal, 1973; Kaimal and Finnigan, 1994). The low-frequency range of these spectra, on the other hand, received disproportionately less attention as this range appears to be non-universal (Kaimal and Finnigan, 1994). The Kansas experiment reported that the spectra of longitudinal (u), lateral (v), and vertical (w) velocity, as well as the spectra of air temperature (T) 'level off' as the wavenumber k decreases (Kaimal and Finnigan, 1994). This levelling-off is featured as reduction in the pre-multiplied spectrum $kE_{ss}(k)$ with decreasing k (i.e. large scales), where $E_{ss}(k)$ is the spectrum of a flow variable $s = u, v, w, T$, and k is the wavenumber. Other measurements in the laboratory and in the atmospheric surface layer (ASL) show that the spectra of u ($E_{uu}(k)$) can have a distinct -1 scaling at low k for near-neutral conditions (Katul and Chu, 1998; Calaf *et al.*, 2013). The k^{-1} scaling in $E_{uu}(k)$ was further conjectured from dimensional analysis (Kader and Yaglom, 1991; Katul *et al.*, 1995), simplified spectral budgets (Tchen, 1953, 1954; Katul *et al.*, 2012; Banerjee and Katul, 2013; Banerjee *et al.*, 2015), and asymptotic matching between outer and inner layers in laboratory boundary layers (Perry and Abell, 1975, 1977; Perry *et al.*, 1986, 1994).

While a -1 scaling has also been identified at low k in $E_{TT}(k)$ in some ASL field experiments under near-neutral, mildly unstable, and mildly stable conditions (Kader and Yaglom, 1991; Katul *et al.*, 1995; Li *et al.*, 2015a), the theoretical conditions promoting its onset have not been considered beyond the z independence argument proposed by Kader and Yaglom (1991), where z is the height above the ground surface. In this argument, when the spectrum of an arbitrary flow variable is normalized by

© 2015 Royal Meteorological Society

'inner-layer' or near-neutral ASL similarity theory variables, then

$$\frac{E_{ss}(k)}{S_*^2 z} = f_{ss}(kz), \tag{1}$$

where $S_* = -\overline{w's'}/u_*$ is an ASL scaling variable, u_* is the friction velocity, and f_{ss} is a universal similarity function. Here, the overline denotes Reynolds averaging and primed quantities denote turbulent fluctuations from the Reynolds averages. For $s = T$, $E_{TT}(k)$ becomes the air temperature spectrum that satisfies

$$\int_0^\infty E_{TT}\left(k'\right) \mathrm{d}k' = \overline{T'T'},$$

and $\overline{T'T'} = \sigma_T^2$ is the air temperature variance. T_* is a characteristic ASL turbulent temperature scale formed by the ratio of the turbulent sensible heat flux ($\overline{w'T'}$) and u_*. For eddies commensurate with the boundary-layer height (i.e. $kz << 1$), $E_{ss}(k)$ becomes independent from z and this independence can be achieved when $f_{ss}(kz) \sim (kz)^{-1}$ resulting in $E_{ss}(k) \sim S_*^2 k^{-1}$ in the near-neutral ASL. In fact, this argument requires that $E_{TT}(k) \sim T_*^2 k^{-1}$ be accompanied by a -1 power-law scaling in the velocity spectra ($E_{uu}(k)$, $E_{vv}(k)$ and $E_{ww}(k)$), though early experiments over water do not support such a claim (Pond *et al.*, 1966). Evidently, other mechanisms that control or modulate the existence of the -1 scaling in $E_{TT}(k)$ must be at play and they need not be tied to the spectrum of the velocity components (particularly $E_{uu}(k)$). Moreover, ASL experiments reporting $E_{TT}(k) \sim k^{-1}$ suggests that the -1 power law extends to $kz \sim 1$, raising questions about the validity of the aforementioned similarity argument. Predicting the onset of a -1 scaling in $E_{TT}(k)$ and its 'disconnect' from the -1 power-law scaling in velocity (particularly $E_{uu}(k)$), and explaining why the -1 scaling in $E_{TT}(k)$ can extend to $kz \sim 1$ when such -1 power-law scaling occurs in $E_{TT}(k)$ frames the scope of this study.

The specific objectives of this study are two-fold. The first is to experimentally explore whether certain atmospheric stability regimes promote a -1 scaling at low k in $E_{TT}(k)$ and what is the wavenumber range over which such power-law scaling holds. The second is to unfold the main causes for the onset of this -1 scaling by employing recently developed spectral and co-spectral budgets (Banerjee and Katul, 2013; Katul et al., 2013; Katul et al., 2014; Banerjee et al., 2015; Li et al., 2015b), where the spectral flux transfer term is 'closed' by a Heisenberg's eddy viscosity concept (Heisenberg, 1948). It is shown that existence of a -1 scaling in $E_{TT}(k)$ is linked to an imbalance between production and dissipation rates in the temperature variance budget, alluded to in previous studies (Hsieh and Katul, 1997; Zilitinkevich *et al.*, 2013). The article is organized as follows: section 2 presents experiments in the ASL over a lake and a grass surface showing the range of atmospheric stability conditions favouring the onset of a -1 scaling in $E_{TT}(k)$; section 3 proposes a theory for the onset of a -1 scaling in $E_{TT}(k)$ using the aforementioned spectral budget; section 4 shows how the model calculations and experimental findings are reconciled, and section 5 concludes the work.

2. Experimental data

Three-dimensional velocity and air temperature time series were sampled at 20 Hz frequency and at four heights (1.65, 2.30, 2.95 and 3.60,m) above an extensive lake surface (Lake Geneva, Switzerland) using four pairs of sonic anemometers (Campbell Scientific Inc., model CSAT3) and open-path gas analyzers (LI-COR, Inc., model LI-7500) from mid August to late October in 2006. The lake, which is one of the largest lakes in Western Europe, is situated on the north side of the Alps (372 m above sea level) and is shared between Switzerland and France. The set-up, data quality controls, and post-processing are presented elsewhere (Vercauteren *et al.*, 2008; Li and Bou-Zeid, 2011; Li *et al.*, 2012). The temperature time series measured by sonic anemometer are corrected for humidity effects (Schotanus *et al.*, 1983) to obtain air temperature time series at each height using the method of Li *et al.* (2012). Calculations of turbulent fluxes follow standard eddy-covariance approaches (Li and Bou-Zeid, 2011; Li *et al.*, 2012) with an averaging interval of 30 min per run. Data with a friction velocity $u_* < 0.01\ \mathrm{m\,s^{-1}}$ and sensible heat flux $|H| < 5\ \mathrm{W\,m^{-2}}$ were excluded from the analysis. Similar to Li *et al.* (2015a), runs where measured turbulent momentum, sensible heat, and latent heat fluxes differed by more than 10% at the four heights were excluded from the analysis here to ensure turbulent fluxes were constant with height in the ASL. In addition, the turbulence intensity has to be smaller than 0.5 to justify the use of Taylor's hypothesis (Stull, 1988) when inferring wavenumbers from time. In addition, similar to Sun *et al.* (2015), highly non-stationary segments were excluded using the quality control described by Foken and Wichura (1996).

Data collected by a continuous meteorological observatory in Wageningen, the Netherlands (7 m above sea level) in 2006 were also used here. The surface is covered with perennial ryegrass (Lolium perenne L.) and rough bluegrass (Poatrivialis L.). The grass is mown weekly during the growing season and has a typical mean height of 0.1 m and a leaf area index of 2.9 $\mathrm{m^2\ m^{-2}}$. The soil is classified as heavy basin clay. Surface heterogeneity is present because of ditches, different grass species in adjacent fields, electricity towers, and a farm some 500 m downwind. Turbulent fluxes of momentum, heat, and mass (H_2O and CO_2) were measured on a lattice tower instrumented with an eddy-covariance system installed at a height of 3.5 m. This system includes a three-dimensional sonic anemometer (3-D Solent, Gill Instruments Ltd., model A1012R2) and an open-path gas analyzer (LI-COR, Inc., model LI-7500), as well as a locally produced fine-wire thermocouple. The data were quality controlled using the eddy-covariance processing toolbox (Sturm *et al.*, 2012). In addition, data with friction velocity $u_* < 0.05\ \mathrm{m\,s^{-1}}$, ASL temperature scale $|T_*| < 0.05\ \mathrm{K}$, or turbulence intensity > 0.5 were excluded from the analysis. To avoid dew conditions, data with relative humidity higher than 90% were also excluded.

For both experiments, spectra are calculated for each 30 min run after linear-detrending following the standard Fourier transform method (Stull, 1988) and are smoothed using a periodic Hamming window without overlap. Dissipation rate of half the temperature variance N_* is calculated using a third-order mixed velocity–temperature structure function $D_{TTu}(r)$ from

$$N_* = -\frac{3}{4}\frac{D_{TTu}(r)}{r}$$

for each run (Kolmogorov, 1941; Monin and Yaglom, 1971) where

$$D_{TTu}(r) = \overline{\left[T\left(x+r\right) - T\left(x\right)\right]^2 \left[u\left(x+r\right) - u\left(x\right)\right]},$$

where r is the separation distance inferred from time series and the mean velocity using Taylor's frozen turbulence hypothesis (Taylor, 1938), and should lie in the inertial subrange. Analysis similar to those in Katul *et al.* (1997) (conducted above a grass surface) indicated that $r = z/2$ was sufficient for the lake data but $r = z/5$ was required for the grass data, where z is the height above the surface. The N_* is also calculated from the second-order temperature structure function. The two estimates of N_* are comparable, as shown in Appendix A.

The 30 min data runs were then separated into eight stability regimes according to the stability parameter $\zeta = z/L$, presented in Table 1, where $L = -u_*^3/(\kappa_v \beta \overline{w'T_v'})$ is the Obukhov length (Obukhov, 1946), $\kappa_v = 0.4$ is the von Kármán constant, $\beta = g/\overline{T_v}$ is the buoyancy parameter, g is the gravitational acceleration, and

© 2015 Royal Meteorological Society

Table 1. The range of ζ, the averaged ζ and the number of 30 min runs in each of the eight stability regimes.

Regime	ζ	Averaged ζ	No. of runs
a	$0.1 < \zeta < 0.2$	0.151	6 (228)
b	$0.05 < \zeta < 0.1$	0.074	23 (339)
c	$0.02 < \zeta < 0.05$	0.034	29 (203)
d	$-0.02 < \zeta < 0.02$	0.007	38 (94)
e	$-0.1 < \zeta < -0.02$	−0.063	97 (444)
f	$-0.5 < \zeta < -0.1$	−0.228	134 (423)
g	$-1 < \zeta < -0.5$	−0.684	40 (30)
h	$-5 < \zeta < -1$	−1.853	44 (11)

In the final column, the first value is from the lake data and the value in parentheses is from the grass data.

T_v is the virtual temperature. When $\zeta < 0$, the ASL is unstable (e.g. over land during the daytime); when $\zeta > 0$, the ASL is stable (e.g. over land during the night-time or over cold water surface). When $\zeta = 0$, the ASL is neutral, though near-neutral conditions are often assumed when $|\zeta| < 0.05$ to 0.1.

3. Theory

As background to the spectral budget for air temperature, the governing Reynolds-averaged equation describing half the temperature variance, $\overline{T'T'}/2$, in an idealized ASL is first considered (Stull, 1988). The idealized ASL flow is assumed to be stationary, planar homogeneous, without subsidence, and characterized by sufficiently high Reynolds and Peclet numbers so that viscous and molecular diffusion effects are negligible except at scales comparable to the Kolmogorov microscale (Stull, 1988). Next, the budget equation for $E_{TT}(k)/2$ for the same idealized ASL state is developed at $k = 1/z$ (Townsend, 1976) using analogies to the temperature variance budget.

3.1. Background and definitions

For the idealized ASL,

$$\frac{1}{2}\frac{\partial \overline{T'T'}}{\partial t} = 0 = -\overline{w'T'}\frac{\partial \overline{T}}{\partial z} + VT - D_m\overline{\left(\frac{\partial T'}{\partial z}\right)^2}, \qquad (2)$$

where t is time and the three terms on the right-hand side represent the production rate of half the temperature variance ($-\overline{w'T'}\mathrm{d}\overline{T}/\mathrm{d}z$), the turbulent transport of half the temperature variance ($VT = -(1/2)\partial\overline{w'T'T'}/\partial z$), and the molecular dissipation rate of half the temperature variance ($D_m\overline{(\partial T'/\partial z)^2} = N_*$). $\partial\overline{T}/\partial z$ is the mean air temperature gradient, $\overline{w'T'}$ is the turbulent sensible heat flux, and D_m is the molecular thermal diffusivity. Again, the overline denotes the Reynolds averaging (or averaging over coordinates of statistical homogeneity) and primed quantities denote turbulent fluctuations from the Reynolds averages.

3.2. A spectral budget

A spectral budget for $E_{TT}(k)/2$ under the same idealized conditions can be written as (Hinze, 1959):

$$\frac{1}{2}\frac{\partial E_{TT}(k)}{\partial t} = 0 = -F_{wT}(k)\frac{\partial \overline{T}}{\partial z} + TR(k) - D_m k^2 E_{TT}(k), \qquad (3)$$

where the three terms on the right-hand side represent the wavenumber-dependent production rate, spectral flux transfer rate (TR), and molecular dissipation rate, respectively. The wavenumber-dependent molecular dissipation rate, when integrated over $[0, \infty]$, yields N_*. Integrating Eq. (3) over $[k, \infty]$ and employing

$$N_* = D_m\int_0^\infty k'^2 E_{TT}(k')\,\mathrm{d}k'$$

gives a simplified spectral budget for N_* at any k (Hinze, 1959; Panchev and Syrakov, 1971):

$$N_*(k) = -\frac{\mathrm{d}\overline{T}}{\mathrm{d}z}\int_k^\infty F_{wT}(k')\,\mathrm{d}k' + \int_k^\infty TR(k')\,\mathrm{d}k' + D_m\int_0^k k'^2 E_{TT}(k')\,\mathrm{d}k', \qquad (4)$$

where the three terms on the right-hand side of represent the production in the range of $[k, \infty]$, the spectral flux transfer in the range of $[k, \infty]$, and the molecular dissipation in the range of $[0, k]$. Here, $F_{wT}(k)$ is the co-spectrum of sensible heat flux ($\overline{w'T'}$) satisfying the normalizing condition

$$\int_0^\infty F_{wT}(k')\,\mathrm{d}k' = \overline{w'T'}.$$

The integral of the spectral flux transfer term is zero (i.e. $\int_0^\infty TR(k')\mathrm{d}k' = 0$) (Hinze, 1959). Note the difference between the *turbulent transport term VT* in Eq. (2) and the *spectral flux transfer term TR* in Eq. (3). The *turbulent transport term VT* describes the transport of temperature variance in physical space and can be finite at any height z though its integral over the entire spatial domain (i.e. boundary-layer height here) is negligible. The *spectral flux transfer term TR* describes the transfer of temperature variance across scales in wavenumber space satisfying the normalizing condition $\int_0^\infty TR(k')\mathrm{d}k' = 0$. When $k \to \infty$ for Eq. (4), $N_* = D_m\int_0^\infty k'^2 E_{TT}(k')\,\mathrm{d}k'$, which recovers the definition of N_*. However, when $k = 0$ for Eq. (4), $N_* = -\overline{w'T'}\mathrm{d}\overline{T}/\mathrm{d}z$, implying that the budget Eq. (2) is in equilibrium, namely, the production rate ($-\overline{w'T'}\mathrm{d}\overline{T}/\mathrm{d}z$) is in balance with the dissipation rate (N_*). This further implies that Eq. (3) (and hence Eq. (4)) is not a simple transformation of Eq. (2). To account for possible imbalances between the production and the dissipation rates of half the temperature variance (i.e. VT) at an arbitrary height z, the N_* on the left-hand side of Eq. (4) must be adjusted by VT so that when $k = 0$, $N_* = -\overline{w'T'}\mathrm{d}\overline{T}/\mathrm{d}z + VT$.

For ASL flows, the focus is on $k = z^{-1}$, namely, when the eddy size is set to the distance from the wall (Townsend, 1976), and Eq. (4) at $k = z^{-1}$ becomes:

$$N_*(z^{-1}) = -\frac{\mathrm{d}\overline{T}}{\mathrm{d}z}\int_{z^{-1}}^\infty F_{wT}(k')\,\mathrm{d}k' + \int_{z^{-1}}^\infty TR(k')\,\mathrm{d}k' + D_m\int_0^{z^{-1}} k'^2 E_{TT}(k')\,\mathrm{d}k', \qquad (5)$$

which is to be evaluated after discussing the parametrization for the production term, the spectral flux transfer term and the molecular dissipation term.

3.3. Parametrization for the production term

To evaluate Eq. (5), it is evident that the spectral shape of $F_{wT}(k)$ in the range of $[z^{-1}, \infty]$ must be determined. For simplicity, it is assumed that $F_{wT}(k)$ follows its classical −7/3 scaling to be consistent with previous co-spectral budget models (Katul *et al.*, 2013, 2014; Li *et al.*, 2015b) and experimental and numerical studies (Lumley, 1967; Kaimal and Finnigan, 1994; Bos *et al.*, 2004; Bos and Bertoglio, 2007), given by:

$$F_{wT}(k) = C'_{wT}\frac{\mathrm{d}\overline{T}}{\mathrm{d}z}\epsilon^{1/3}k^{-7/3}, \qquad (6)$$

© 2015 Royal Meteorological Society

where ϵ is the mean turbulent kinetic energy dissipation rate and

$$C'_{wT} = QC_{wT} = \left[1 - \frac{1}{1-C_{\rm IT}}\frac{C_T}{C_o}\frac{\zeta}{\{\phi_{\rm m}(\zeta)-\zeta\}}\right]C_{wT}. \quad (7)$$

C_{wT} (≈ 0.15) is the co-spectral similarity constant for near-neutral conditions (Kaimal and Finnigan, 1994) and Q represents the impact of atmospheric stability on the co-spectral similarity constant (Katul *et al.*, 2013, 2014; Li *et al.*, 2015b). $C_{\rm IT}$ (≈ 0.6) is a constant associated with isotropization of the production term in the sensible heat flux budget whose value can be determined using Rapid Distortion Theory in homogeneous turbulence (Launder *et al.*, 1975; Pope, 2000). C_o and C_T are the Kolmogorov and Kolmogorov–Obukhov–Corrsin constants for vertical velocity and air temperature spectra, respectively. For a one-dimensional interpretation of k, their common values are $C_o = 0.65$ and $C_T = 0.8$ (Sreenivasan, 1995; Sreenivasan and Antonia, 1997; Ishihara *et al.*, 2002; Chung and Matheou, 2012). $\phi_{\rm m}(\zeta) = [\kappa_v z/u_*](\mathrm{d}\overline{u}/\mathrm{d}z)$ is the stability correction function for the mean velocity gradient ($\mathrm{d}\overline{u}/\mathrm{d}z$), which is only a function of ζ (Obukhov, 1946; Monin and Obukhov, 1954; Businger and Yaglom, 1971). Using Eq. (6), the first term on the right-hand side of Eq. (5) can now be evaluated as

$$-\frac{\mathrm{d}\overline{T}}{\mathrm{d}z}\int_{z^{-1}}^{\infty} F_{wT}(k)\,\mathrm{d}k = -\frac{3}{4}C'_{wT}\epsilon^{\frac{1}{3}}z^{\frac{4}{3}}\left(\frac{\mathrm{d}\overline{T}}{\mathrm{d}z}\right)^2. \quad (8)$$

3.4. Parametrization for the spectral flux transfer term

To evaluate the second term in Eq. (5), Heisenberg's eddy viscosity concept is employed (Heisenberg, 1948; Hinze, 1959):

$$\int_k^{\infty} TR\left(k'\right)\mathrm{d}k' = \frac{1}{2}\int_k^{\infty} D_{\rm t}\left(k'\right)\mathrm{d}k'\int_0^k 2k'^2E_{TT}\left(k'\right)\mathrm{d}k', \quad (9)$$

where $D_{\rm t}\left(k'\right)$ is a wavenumber-dependent turbulent thermal diffusivity related to the turbulent eddy viscosity $\nu_{\rm t}(k')$ using a turbulent Prandtl number ($Pr_{\rm t}$, the ratio of turbulent eddy viscosity and turbulent thermal diffusivity) given by

$$D_{\rm t}\left(k'\right) = Pr_{\rm t}^{-1}\nu_{\rm t}(k') = Pr_{\rm t}^{-1}C_{\rm H}\sqrt{\frac{E_{\rm TKE}(k')}{k'^3}}. \quad (10)$$

Here, $Pr_{\rm t}^{-1} = Pr_{\rm t,neu}^{-1}Q$ (Katul *et al.*, 2013, 2014; Li *et al.*, 2015b), where $Pr_{\rm t,neu}$ is the turbulent Prandtl number under neutral conditions (≈ 0.74), $C_{\rm H}$ is the Heisenberg constant ($\approx (8/9)C_o^{-3/2}$ for isotropic conditions; Schumann, 1994) and $E_{\rm TKE}(k)$ is the turbulent kinetic energy spectrum. Note in Eq. (9) that $TR(0) = 0$ and $TR(\infty) = 0$ are enforced by virtue of the closure model construction (Hinze, 1959). When $E_{\rm TKE}(k)$ follows its classical Kolmogorov $-5/3$ scaling in the range of $[z^{-1}, \infty]$ (Kolmogorov, 1941), that is, $E_{\rm TKE}(k) = C_o\epsilon^{2/3}k^{-5/3}$, Eq. (10) leads to

$$\int_{z^{-1}}^{\infty} D_{\rm t}(k')\mathrm{d}k' = \frac{3}{4}Pr_{\rm t}^{-1}C_{\rm H}C_o^{\frac{1}{2}}\epsilon^{\frac{1}{3}}z^{\frac{4}{3}}. \quad (11)$$

Here, exponential corrections to $k^{-5/3}$ due to viscous effects are ignored for simplicity given the assumed high Reynolds number (i.e. large separation in scales between z and the Kolmogorov microscale η) though these corrections can be included. Also, intermittency corrections to the $k^{-5/3}$ within the inertial subrange scaling are usually small for second-order statistics such as spectra as discussed elsewhere (Sreenivasan and Antonia, 1997) and are ignored here for simplicity, though they can also be accommodated. With these approximations,

$$\int_{z^{-1}}^{\infty} TR(k')\mathrm{d}k' = \frac{3}{4}Pr_{\rm t}^{-1}C_{\rm H}C_o^{\frac{1}{2}}\epsilon^{\frac{1}{3}}z^{\frac{4}{3}}\int_0^{z^{-1}} k'^2E_{TT}(k')\mathrm{d}k'. \quad (12)$$

3.5. Parametrization for the molecular dissipation term

The ratio of the transfer to the molecular dissipation terms in Eq. (5) is:

$$\frac{\int_{z^{-1}}^{\infty} TR(k')\mathrm{d}k'}{D_{\rm m}\int_0^{z^{-1}} k'^2E_{TT}(k')\mathrm{d}k'} = \frac{\int_{z^{-1}}^{\infty} D_{\rm t}(k')\mathrm{d}k'}{D_{\rm m}} = \frac{3}{4}C_{\rm H}C_o^{\frac{1}{2}}\kappa_v^{-\frac{1}{3}}\frac{\nu_{\rm m}}{D_{\rm m}}Pr_{\rm t}^{-1}\phi_\epsilon^{1/3}Re, \quad (13)$$

where $Re = u_*z/\nu_{\rm m}$ is the Reynolds number, $\nu_{\rm m}$ is the kinematic molecular viscosity and $\phi_\epsilon = \epsilon\kappa_v z/u_*^3$ is the normalized dissipation rate for turbulent kinetic energy. For a sufficiently high Re, the molecular dissipation term is much smaller than the transfer term and hence can be ignored at $k = 1/z$ (Banerjee and Katul, 2013; Banerjee *et al.*, 2015).

3.6. Evaluation of the temperature spectrum

Given these approximations for all three terms on the right-hand side of Eq. (5) and $N_* = -\overline{w'T'}\mathrm{d}\overline{T}/\mathrm{d}z + VT$, it can be shown that

$$-\overline{w'T'}\frac{\mathrm{d}\overline{T}}{\mathrm{d}z} + VT = -\frac{3}{4}C'_{wT}\epsilon^{\frac{1}{3}}z^{\frac{4}{3}}\left(\frac{\mathrm{d}\overline{T}}{\mathrm{d}z}\right)^2 + \frac{3}{4}Pr_{\rm t}^{-1}C_{\rm H}C_o^{\frac{1}{2}}\epsilon^{\frac{1}{3}}z^{\frac{4}{3}}\int_0^{z^{-1}} k'^2E_{TT}(k')\mathrm{d}k', \quad (14)$$

which can be arranged to yield

$$\int_0^{z^{-1}} k'^2E_{TT}(k')\mathrm{d}k' = \frac{\frac{3}{4}\kappa_v^{-\frac{4}{3}}C'_{wT}\phi_T{}^2 + \phi_T\phi_\epsilon^{-\frac{1}{3}} + \phi_{VT}\phi_\epsilon^{-\frac{1}{3}}}{\frac{3}{4}Pr_{\rm t}^{-1}C_{\rm H}C_o^{\frac{1}{2}}\kappa_v^{\frac{2}{3}}}\frac{T_*^2}{z^2}, \quad (15)$$

where $\phi_T(\zeta) = [\kappa_v z/T_*](\mathrm{d}\overline{T}/\mathrm{d}z)$ is the stability correction function for the mean air temperature gradient, and $T_* = -\overline{w'T'}/u_*$ is again the temperature scaling parameter for the ASL. It can be shown that, by definition, $\phi_T(\zeta)/\phi_{\rm m}(\zeta) = Pr_{\rm t}(\zeta)$. The ϕ_{VT} is a normalized imbalance between production and dissipation rates, defined as:

$$\phi_{VT} = \frac{\kappa_v z}{u_*T_*^2}VT = \phi_{N_*}(\zeta) - \phi_T(\zeta). \quad (16)$$

where $\phi_{N_*}(\zeta) = N_*\kappa_v z/(u_*T_*^2)$ is the normalized dissipation rate for half the temperature variance.

Similar to the approach used in Banerjee *et al.* (2015) for $E_{uu}(k)$, it is assumed that the solution to the air temperature spectrum follows a power law whose form is $E_{TT}(k) = ak^b$ in the range of $[0, z^{-1}]$, where a is the spectral similarity constant and b is the scaling exponent to be determined from the spectral budget next. With this assumed shape, Eq. (15) is reduced to:

$$\frac{a}{b+3}\frac{1}{z^{b+3}} = \frac{\frac{3}{4}\kappa_v^{-\frac{4}{3}}C'_{wT}\phi_T{}^2 + \phi_T\phi_\epsilon^{-\frac{1}{3}} + \phi_{VT}\phi_\epsilon^{-\frac{1}{3}}}{\frac{3}{4}Pr_{\rm t}^{-1}C_{\rm H}C_o^{\frac{1}{2}}\kappa_v^{\frac{2}{3}}}\frac{T_*^2}{z^2} = \frac{\phi_a}{2}\frac{T_*^2}{z^2}, \quad (17)$$

where, for convenience, ϕ_a is given as

$$\phi_a = 2\left(\frac{\frac{3}{4}\kappa_v^{-\frac{4}{3}}C'_{wT}\phi_T{}^2 + \phi_T\phi_\epsilon^{-\frac{1}{3}} + \phi_{VT}\phi_\epsilon^{-\frac{1}{3}}}{\frac{3}{4}Pr_{\rm t}^{-1}C_{\rm H}C_o^{\frac{1}{2}}\kappa_v^{\frac{2}{3}}}\right) = \phi_{a_1} + \phi_{a_2} + \phi_{a_3}. \quad (18)$$

© 2015 Royal Meteorological Society

That is, ϕ_a arises from the superposition of three processes given as

$$\phi_{a_1} = 2\left(\frac{\frac{3}{4}\kappa_v^{-\frac{4}{3}} C'_{wT}\phi_T{}^2}{\frac{3}{4}Pr_t^{-1}C_H C_o^{\frac{1}{2}}\kappa_v^{\frac{2}{3}}}\right), \quad (19)$$

$$\phi_{a_2} = 2\left(\frac{\phi_T\phi_\epsilon^{-\frac{1}{3}}}{\frac{3}{4}Pr_t^{-1}C_H C_o^{\frac{1}{2}}\kappa_v^{\frac{2}{3}}}\right), \quad (20)$$

$$\phi_{a_3} = 2\left(\frac{\phi_{VT}\phi_\epsilon^{-\frac{1}{3}}}{\frac{3}{4}Pr_t^{-1}C_H C_o^{\frac{1}{2}}\kappa_v^{\frac{2}{3}}}\right). \quad (21)$$

If ϕ_a is independent from z, then polynomial matching in Eq. (17) yields $b = -1$ and a spectral similarity constant $a = \phi_a T_*^2$, so that $E_{TT} = \phi_a T_*^2 k^{-1}$. That is, the temperature spectra must follow a -1 scaling in the range of $[0, z^{-1}]$ but only when ϕ_a is independent from z. With this derivation, the objective of identifying atmospheric stability conditions promoting or suppressing the -1 power-law scaling in $E_{TT}(k)$ can be readily addressed by analyzing conditions promoting z independence in ϕ_a. Contributions from ϕ_{a_1}, ϕ_{a_2}, and ϕ_{a_3} to ϕ_a across various ζ ranges are now considered and discussed using the two aforementioned experiments.

4. Results

Figures 1 and 2 present the averaged $E_{TT}(k)$ for each of the eight stability regimes listed in Table 1 using the lake and grass data. Also shown are the -1 scaling (in the low-wavenumber range) in all panels and the $-5/3$ scaling (in the high-wavenumber range) in (a) for illustration. Following Kader and Yaglom (1991) and Katul *et al.* (1995) who showed that $\phi_a \approx 0.9$ under near-neutral conditions, the black lines in Figures 1 and 2 correspond to $E_{TT}(k) = 0.9T_*^2 k^{-1}$. Measured $E_{TT}(k)$ in (a)–(e) (i.e. $-0.1 < \zeta < 0.2$) exhibit a distinct -1 scaling at the low k and are in acceptable agreement with $\phi_a = 0.9$. A -1 scaling is also observed in $E_{uu}(k)$ over the same stability range (not shown) while the energy spectra of the vertical velocity, $E_{ww}(k)$, saturates to a near-constant value at low k (Li *et al.*, 2015a). This saturation in $E_{ww}(k)$ indicates that the measurements are from the 'eddy surface layer' according to Drobinski *et al.* (2004). In addition, the transition between the -1 and the $-5/3$ scaling occurs in the vicinity of $kz = 1$ supporting the evaluation of the spectral budget at $k = z^{-1}$ (Eq. (5)) and assuming inertial subrange scaling applies for $kz > 1$ consistent with the results in Kader and Yaglom (1991). However, for (f)–(h), the range of k following a -1 scaling is diminished and measured $E_{TT}(k)$ at low k appreciably deviate from $E_{TT}(k) = 0.9T_*^2 k^{-1}$. It is also noted here that the scaling in the inertial subrange seems to deviate from its classical $-5/3$ value under near-neutral conditions (e.g. regimes *d* and *e*), which is consistent with other long-term field measurements (Grachev *et al.*, 2013).

Figure 3 shows variations of ϕ_a and its three components, ϕ_{a_1}, ϕ_{a_2} and ϕ_{a_3}, when $-0.1 < \zeta < 0.2$ (i.e. in stability regimes where the -1 scaling is observed). To calculate ϕ_{a_1} and ϕ_{a_2}, the Businger–Dyer relations for $\phi_m(\zeta)$ are assumed (Businger *et al.*, 1971; Businger, 1988). The $\phi_T(\zeta)$ is calculated as $\phi_T(\zeta) = Pr_t(\zeta)\phi_m(\zeta) = Pr_{t,neu}Q^{-1}\phi_m(\zeta)$, where Q is determined from Eq. (7). This aforementioned determination of Q must be viewed as a simplification whose (minor) consequences are explored in Appendix B. In addition, the budget equation for the turbulent kinetic energy is assumed to be in equilibrium (Katul *et al.*, 2013, 2014; Li *et al.*, 2015b) so that $\phi_\epsilon(\zeta) = \phi_m(\zeta) - \zeta$ (Banerjee *et al.*, 2015, gives experimental evaluation of this assumption). The ϕ_{a_3} is determined for reference so that ϕ_a, the sum of ϕ_{a_1}, ϕ_{a_2} and ϕ_{a_3}, is 0.9 consistent with the value in Figures 1 and 2.

It is evident from Figure 3 that ϕ_{a_1} and ϕ_{a_2} are large but roughly cancel each other. Nonetheless, the sum of ϕ_{a_1} and ϕ_{a_2} still exhibits a weak dependence on ζ and hence on z. Consequently, if ϕ_{a_3} is assumed to be 0 (i.e. $\phi_{VT} = 0$), $\phi_a = \phi_{a_1} + \phi_{a_2}$ exhibits a weak dependence on z and the resulting $E_{TT}(k)$ from Eq. (17) cannot strictly follow a -1 scaling for k within $[0, z^{-1}]$. Within the limits of the theory here, the only mechanism that counters such z dependence is a non-zero ϕ_{a_3}. The ϕ_{a_3} must slightly increase with increasing instability as shown in Figure 3 to yield a ϕ_a independent of z for near-neutral stability conditions. As such,

$$\phi_{VT} = \phi_{a_3}\left(\frac{2\,\phi_\epsilon^{-\frac{1}{3}}}{\frac{3}{4}Pr_t^{-1}C_H C_o^{\frac{1}{2}}\kappa_v^{\frac{2}{3}}}\right)^{-1}, \quad (22)$$

cannot be 0 but must increase as ζ decreases (i.e. as the atmosphere becomes unstable).

Although the -1 scaling of $E_{TT}(k)$ is diminished or absent altogether in stability regimes *f* to *h* (Figures 1 and 2), analysis similar to Figure 3 is conducted over the range of ζ covered by these unstable regimes simply to illustrate the requirement for ϕ_{a_3} (and hence ϕ_{VT}) if a -1 scaling were to hold for these unstable regimes. Figure 4 shows the variations of ϕ_a and its three different components, ϕ_{a_1}, ϕ_{a_2}, and ϕ_{a_3}, when $-5 < \zeta < -0.1$. Again, ϕ_{a_3} is calculated so that ϕ_a (the sum of ϕ_{a_1}, ϕ_{a_2}, and ϕ_{a_3}) equals to 0.9. As can be seen, the sum of ϕ_{a_1} and ϕ_{a_2} depends on ζ and hence on z, especially when $\zeta > -1$. In addition, the sum of ϕ_{a_1} and ϕ_{a_2} approaches 0 at small ζ. To achieve a continuous ϕ_a that is also independent of z, ϕ_{a_3} must increase significantly with increasing $-\zeta$ (i.e. as the atmosphere becomes more unstable). As a result, ϕ_{VT} must increase concomitantly as $-\zeta$ increases.

Figure 5 shows calculated ϕ_{VT} from ϕ_{a_3} promoting -1 scaling (Eq. (22)), as compared to estimated ϕ_{VT} from Eq. (16) with N_* inferred from the third-order mixed velocity–temperature structure function $D_{TTu}(r)$. Similar results are obtained with N_* inferred from second-order temperature structure function (Appendix A). The experiments here suggest an increasing ϕ_{VT} as ζ decreases when $-0.1 < \zeta < 0.2$ (regimes *a* to *e*), which is because ϕ_{VT} is mostly negative under stable conditions but switches to positive under unstable conditions over this stability range. Hence, the experiments here confirm that ϕ_{VT} is non-zero and can vary with ζ. A ϕ_{VT} switching sign in the near-neutral limit as ζ crosses from unstable to stable conditions (and conversely) appears necessary for the existence of a -1 scaling in $E_{TT}(k)$ even when the ASL flow is idealized. The agreement between the model calculations and experimental results during $0.1 < \zeta < 0.2$ (regime *a*) seems to be satisfactory but poorer than in the other regimes where the -1 scaling exists, which is probably also due to the relatively smaller number of segments (particularly the lake data) in this regime.

When $-5 < \zeta < -0.1$ (regimes *f* to *h*), the conditions promoting the -1 scaling in $E_{TT}(k)$ are no longer satisfied. The experiments indicate that the normalized imbalance between production and dissipation rates of half the temperature variance (ϕ_{VT}) fall short of what is needed to maintain a -1 power-law scaling for the stability range of $-5 < \zeta < -0.1$. This is the main reason why a -1 power-law scaling is absent for such stability regimes. The $-5 < \zeta < -0.5$ are not presented in Figure 5 since they show an even larger discrepancy between conditions promoting -1 scaling in $E_{TT}(k)$ and the experimental data as compared to those when $-0.5 < \zeta < -0.1$.

5. Discussion and conclusions

The stability conditions promoting or suppressing the -1 power-law scaling in the low k range of $E_{TT}(k)$ are examined experimentally using ASL data collected above a lake and a grass surface and theoretically using simplifications to an air temperature spectral budget. In agreement with the theoretical predictions, the experiments reveal a -1 scaling law for $E_{TT}(k)$ under mildly unstable to mildly stable conditions (when

© 2015 Royal Meteorological Society

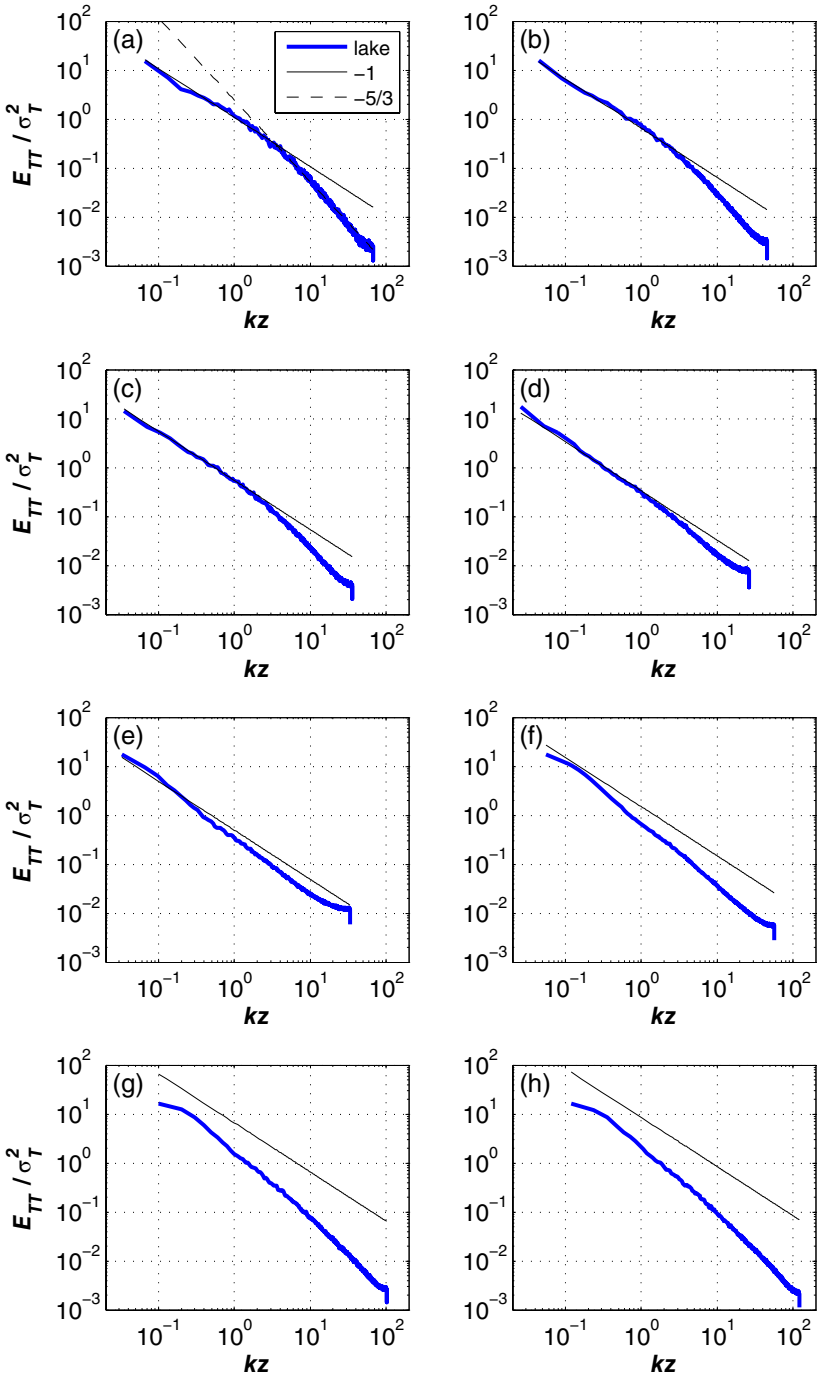

Figure 1. The measured normalized spectra of air temperature ($E_{TT}(k)$) for the eight stability regimes from the lake data. (a)–(h) correspond to the stability regimes designated as *a* to *h* in Table 1. All spectra are averaged over all segments included in each stability regime. The black lines are $E_{TT} = 0.9T_*^2 k^{-1}$ (i.e. $\phi_a = 0.9$). The $E_{TT}(k)$ in (a)–(e) show a distinct -1 scaling in the low-wavenumber range and the transitions between -1 and $-5/3$ scaling occur in the vicinity of $kz = 1$.

$-0.1 < \zeta < 0.2$). As instability increases (when $-5 < \zeta < -0.1$), the measured -1 scaling in $E_{TT}(k)$ diminishes or censors consistent with theoretical expectations. The theory underscores the significant role of ϕ_{VT}, the normalized imbalance between the production and dissipation rates of half the temperature variance, in controlling the -1 scaling. When $-0.1 < \zeta < 0.2$, ϕ_{VT} estimated from experiments shows a weak dependence on z, which results in a z-independent ϕ_a and a -1 scaling in the low k range of $E_{TT}(k)$. When $-5 < \zeta < -0.1$, ϕ_{VT} estimated from experiments appears insensitive to z/L, thereby suppressing the onset of a -1 scaling in $E_{TT}(k)$.

The results presented here have two implications. First, the fact that ϕ_{VT} plays a role in the -1 scaling of $E_{TT}(k)$ implies that possible connections between $E_{uu}(k)$ and $E_{TT}(k)$ are more complicated than what prior dimensional analysis may suggest. Banerjee and Katul (2013) and Banerjee *et al.* (2015) examined the -1 scaling in $E_{uu}(k)$ using a similar approach but did not retain a finite *turbulent transport term* in their budget equation for turbulent kinetic energy, suggesting an insignificant role of the imbalance between the production and dissipation rates of turbulent kinetic energy in controlling the existence of -1 scaling of $E_{uu}(k)$. As a result, the existence of -1 scaling in $E_{uu}(k)$ does not automatically imply a -1 scaling in $E_{TT}(k)$ at low k. This might explain why some experiments (including the lake/grassland experiments presented here) reported concurrent -1 scaling in $E_{uu}(k)$ and $E_{TT}(k)$ but not other experiments (Pond *et al.*, 1966). The spectral/co-spectral budgets proposed here, by virtue of their formulation, explain why a -1 scaling in $E_{TT}(k)$ must extend to $kz \sim 1$ whereas previous dimensional analysis assumes the -1 scaling holds for $kz << 1$ (Kader and Yaglom, 1991).

Second, given that

$$\int_0^\infty E_{TT}\left(k'\right) \mathrm{d}k' = \overline{T'T'} = \sigma_T^2,$$

© 2015 Royal Meteorological Society

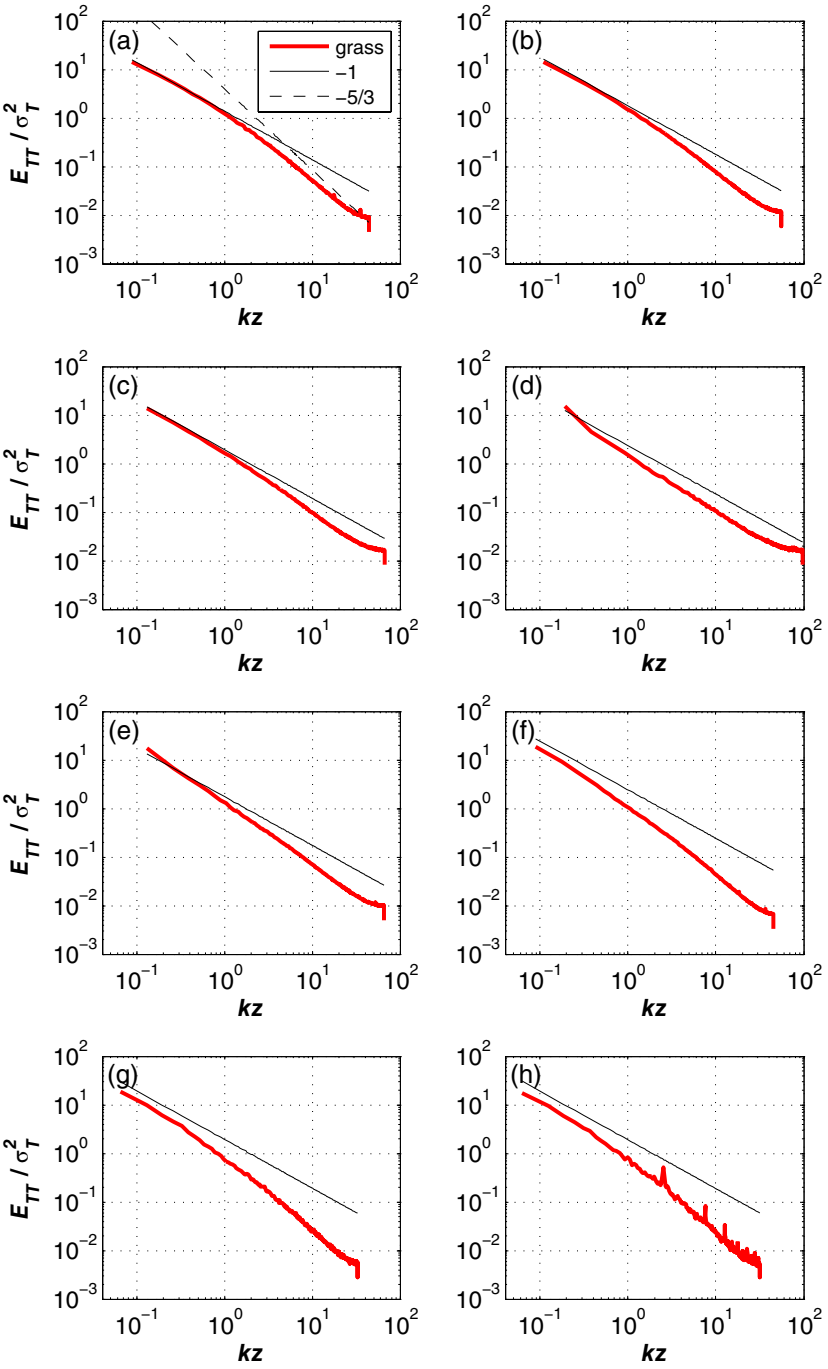

Figure 2. As Figure 1 but for the grass data.

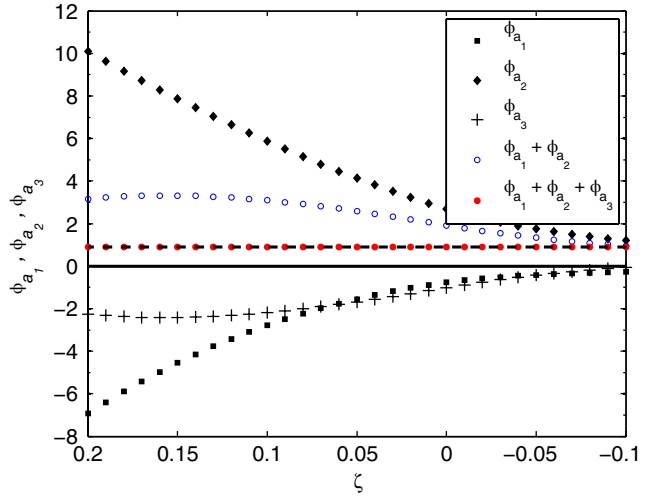

Figure 3. The variations of ϕ_{a_1}, ϕ_{a_2}, and ϕ_{a_3} with ζ. The dashed line corresponds to a value of 0.9. The range of ζ shown here includes regimes *a* to *e* in Table 1.

the -1 scaling in the $E_{TT}(k)$ will result in a dependence of σ_T on the scale that characterizes the largest turbulent disturbances ($kz << 1$) such as the atmospheric boundary-layer height. A similar result but for σ_u has been presented elsewhere (Banerjee and Katul, 2013; Banerjee *et al.*, 2015). A dependence of σ_T on the atmospheric boundary-layer height might explain the large scatter of σ_T/T_* under near-neutral conditions, especially when the sensible heat flux or T_* is finite (i.e. not too small). Future studies involving comparisons between $E_{TT}(k)$ and the spectra of other scalars such as q (i.e. water vapour) and CO_2 might shed light on how the -1 scaling in the $E_{TT}(k)$ affects scalar similarity and flux-variance relations.

The -1 scaling examined here is different from the classical -1 scaling in the 'viscous–convective' subrange at large Schmidt or Prandtl numbers (Davidson *et al.*, 2012). The -1 scaling in E_{TT} here describes the low-wavenumber range (from $k = 0$ to $k = 1/z$, where z is the height above the ground) and is not connected to a large molecular Prandtl number (in fact the Prandtl number of the air is only about 0.71); while the -1 scaling in the viscous–convective subrange spans from $k\eta = 0.2$ to $k\eta = 1$ (Bos and Bertoglio, 2013) and requires a molecular

© 2015 Royal Meteorological Society

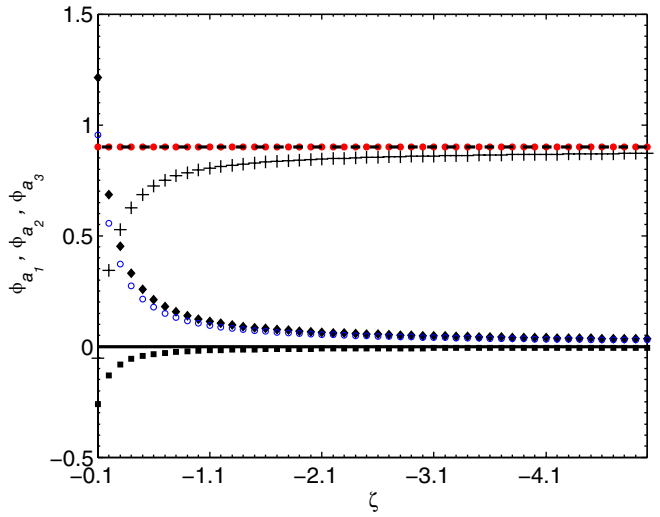

Figure 4. As Figure 3, but for regimes *f* to *h* in Table 1.

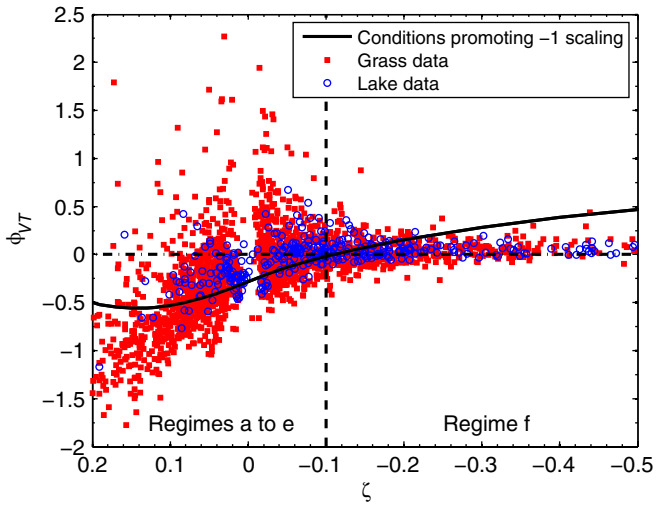

Figure 5. The normalized imbalance between production and dissipation rate of half the temperature variance (ϕ_{VT}). The line is calculated using Eq. (22) with ϕ_{a_3} shown in Figures 3 and 4. The circles (squares) are estimated from the lake (grassland) data using Eq. (16) with N_* inferred from the third-order mixed velocity–temperature structure function $D_{TTu}(r)$.

Schmidt or Prandtl number to be sufficiently large. Lastly, it is noted that although linear-detrending and stationarity tests have been applied, some residual non-stationarity effect might still exist and impact the scaling of temperature spectra at low frequencies. Future investigations using measurements collected from controlled lab experiments are recommended.

Acknowledgements

DL acknowledges support from the NOAA (US Department of Commerce) grant NA08OAR4320752 and the Carbon Mitigation Initiative at Princeton University, sponsored by BP. The statements, findings, and conclusions are those of the authors and do not necessarily reflect the views of the NOAA, the US Department of Commerce or BP. GK acknowledges support from the National Science Foundation (NSF-EAR-1344703), the US Department of Energy (DOE) through the office of Biological and Environmental Research (BER) Terrestrial Ecosystem Science (TES) Program (DE-SC0006967 and DE-SC0011461). PG acknowledges support from the NASA grant NNX14AI36G. We thank Professor Marc Parlange for sharing the lake data, which were collected by his Environmental Fluid Mechanics and Hydrology Laboratory at the École Polytechnique Fédérale de Lausanne. We also would like to thank Bert Heusinkveld for providing the grass data collected at Wageningen University.

Appendix A

Computation of dissipation rates from experimental data

In this study, two methods are used to calculate the dissipation rate of half the temperature variance N_*. The first method calculates N_* from the second-order temperature structure function following $N_* = -(0.3125)\{D_{TT}(r)/r^{2/3}\}\epsilon^{1/3}$ and the second method calculates N_* from the third-order mixed velocity–temperature structure function $D_{TTu}(r)$ following $N_* = -(3/4)\{D_{TTu}(r)\}/r$ (Stull, 1988) for each run, where r is the separation distance aligned along the mean wind direction and inferred from Taylor's frozen turbulence hypothesis (Taylor, 1938),

$$D_{TT}(r) = \overline{\{T(x+r) - T(x)\}^2}$$
$$\text{and } D_{TTu}(r) = \overline{\{T(x+r) - T(x)\}^2 \{u(x+r) - u(x)\}}.$$

Estimation of N_* from the second-order structure function requires the dissipation rate of turbulent kinetic energy ϵ, which can be also computed from either second-order or third-order longitudinal velocity structure functions (Hsieh and Katul, 1997).

Figure A1 shows comparisons of normalized N_* (ϕ_{N*}) and ϵ (ϕ_ϵ) estimated from second-order and third-order structure functions. Despite some scatter, especially for the grass data, it is clear that the two estimates generally agree with each other, consistent with other findings (Bou-Zeid *et al.*, 2010). When N_* and ϵ estimated from second-order structure functions are used, conditions promoting the k^{-1} scaling are still satisfied when $-0.1 < \zeta < 0.2$ (not shown here but can be inferred from Figures 5 and A1).

The scatter seen in the grass data in Figure A1 is probably due to a combination of limited inertial subrange and high turbulence intensity. For the grass data, $r = z/5$ is chosen, as compared to $r = z/2$ for the lake data. This is because D_{TT} and D_{uu} clearly do not follow the $r^{-2/3}$ scaling at $r = z/2$ (not shown) and hence a smaller r has to be used to be in the inertial subrange. Given that the averaging path of a sonic anemometer is about 15 cm, the inertial subrange is hence relatively narrow for the grass data, which makes it more challenging to estimate dissipation rates from structure functions. In addition, the high turbulence intensities also modulate the relationship between dissipation rates from structure functions (e.g. the coefficient 0.3125 in the calculation of N_* from D_{TT} depends on the turbulent intensity, as shown in Hsieh and Katul, 1997). In this study, the turbulence intensity is restricted to be smaller than 0.5 as recommended by Stull (1988) to justify the use of Taylor's frozen turbulence hypothesis. When a more stringent criterion is used (e.g. the turbulence intensity needs to be smaller than 0.25), the scatter is significantly reduced (not shown here). It is stressed that, despite the scatter, the experimental data agree with model calculations fairly well, as can be seen from Figure 5.

Appendix B

Computation of Q in the co-spectral budget model

In the co-spectral budget model used to estimate the production term (Eq. (6)), it is assumed that the budget equation for half the temperature variance is in equilibrium or $VT = 0$ so as to obtain Q. The Q is needed for computing C'_{wT} and Pr_t. To assess the effects of a non-zero VT on Q, a revised (and lengthy) expression for Q is derived by retaining VT. This expression is given as

$$Q = \left\{1 - \frac{1}{1-C_{IT}} \frac{C_T}{C_o} \frac{\zeta}{(\phi_m(\zeta) - \zeta)} \left(1 + \frac{\phi_{VT}}{\phi_T}\right)\right\}. \quad \text{(B1)}$$

© 2015 Royal Meteorological Society

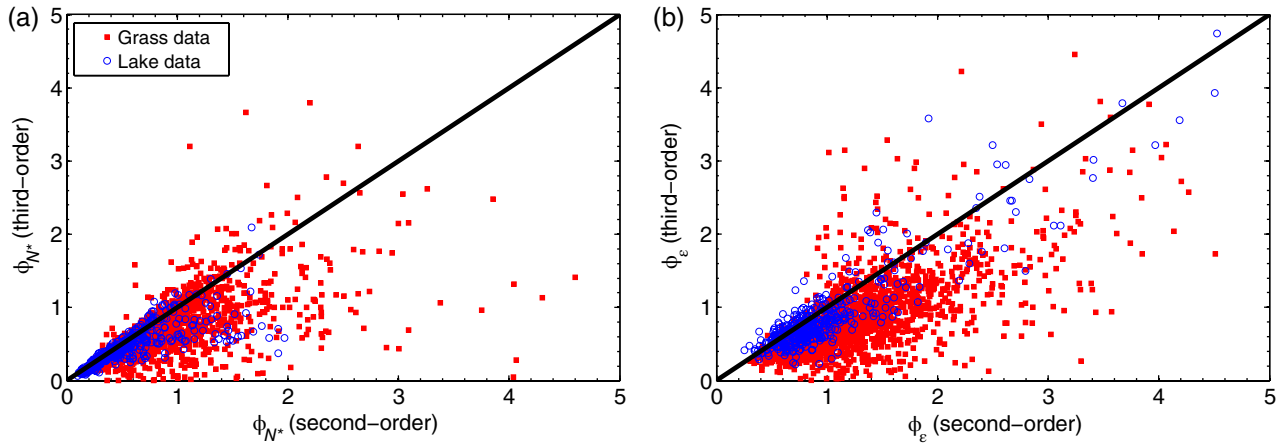

Figure A1. The comparison of (a) ϕ_{N*} and (b) ϕ_ϵ from second-order and third-order structure functions.

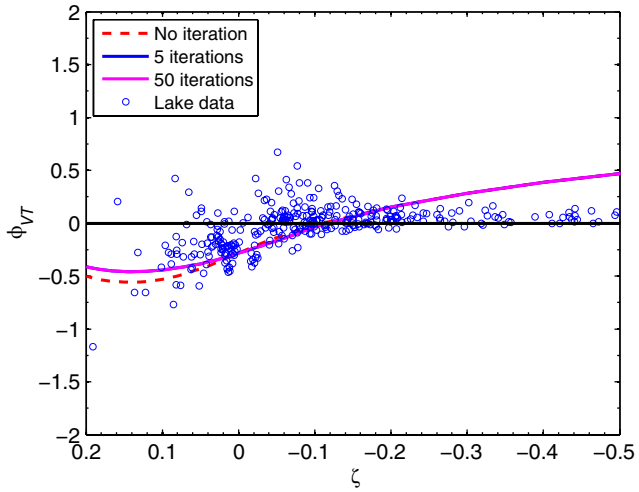

Figure B1. The normalized imbalance between production and dissipation rates of half the temperature variance (ϕ_{VT}). The lines are calculations using multiple iterations.

It is clear from Eq. (B1) that the new Q further depends on the ratio of ϕ_{VT}/ϕ_T, suggesting that a non-zero ϕ_{VT} alters the atmospheric stability impact on Pr_t and C'_{wT} from what was previously assumed. As a result, ϕ_{a_1}, ϕ_{a_2}, and ϕ_{a_3} are now all dependent on ϕ_{VT} and solving $\phi_{a_1} + \phi_{a_2} + \phi_{a_3} = 0.9$ to obtain ϕ_{VT} requires an iterative procedure. Figure B1 shows the calculation of ϕ_{VT} using multiple iterations compared to the lake data when $-0.5 < \zeta < 0.2$ (i.e. similar to Figure 5). As can be seen, the iterations converge very quickly since the results with five iterations are almost identical to those with 50 iterations (the two lines overlap on Figure B1). The revised calculations are not significantly impacted and remain consistent with measurements over the stability range $-0.1 < \zeta < 0.2$ where the -1 scaling is observed.

References

Banerjee T, Katul G. 2013. Logarithmic scaling in the longitudinal velocity variance explained by a spectral budget. *Phys. Fluids* **25**: 125106.

Banerjee T, Katul GG, Salesky ST, Chamecki M. 2015. Revisiting the formulations for the longitudinal velocity variance in the unstable atmospheric surface layer. *Q. J. R. Meteorol. Soc.* **141**: 1699–1711, doi: 10.1002/qj.2472.

Bos W, Bertoglio J. 2007. Inertial range scaling of scalar flux spectra in uniformly sheared turbulence. *Phys. Fluids* **19**: 25104–25111.

Bos WJ, Bertoglio JP. 2013. Lagrangian Markovianized field approximation for turbulence. *J. Turbul.* **14**: 99–120.

Bos W, Touil H, Shao L, Bertogli J. 2004. On the behavior of the velocity-scalar cross correlation spectrum in the inertial range. *Phys. Fluids* **16**: 3818–3823.

Bou-Zeid E, Higgins C, Huwald H, Parlange M, Meneveau C. 2010. Field study of the dynamics and modelling of subgrid scale turbulence in a stable atmospheric surface layer over a glacier. *J. Fluid Mech.* **665**: 480–515.

Businger JA. 1988. A note on the Businger–Dyer profiles. *Boundary-Layer Meteorol.* **42**: 145–151.

Businger JA, Yaglom AM. 1971. Introduction to Obukhov's paper on 'Turbulence in an atmosphere with a non-uniform temperature'. *Boundary-Layer Meteorol.* **2**: 3–6.

Businger JA, Wyngaard JC, Izumi Y, Bradley EF. 1971. Flux-profile relationships in the atmospheric surface layer. *J. Atmos. Sci.* **28**: 181–191.

Calaf M, Hultmark M, Oldroyd H, Simeonov V, Parlange M. 2013. Coherent structures and the k^{-1} spectral behaviour. *Phys. Fluids* **25**: 125107, doi: 10.1063/1.4834436.

Chung D, Matheou G. 2012. Direct numerical simulation of stationary homogeneous stratified sheared turbulence. *J. Fluid Mech.* **696**: 434–467.

Davidson PA, Kaneda Y, Sreenivasan KR. 2012. *Ten Chapters in Turbulence*. Cambridge University Press: Cambridge, UK.

Drobinski P, Carlotti P, Newsom RK, Banta RM, Foster RC, Redelsperger JL. 2004. The structure of the near-neutral atmospheric surface layer. *J. Atmos. Sci.* **61**: 699–714.

Foken T, Wichura B. 1996. Tools for quality assessment of surface-based flux measurements. *Agric. Meteorol.* **78**: 83–105.

Grachev A, Andreas E, Fairall C, Guest P, Persson POG. 2013. The critical Richardson number and limits of applicability of local similarity theory in the stable boundary layer. *Boundary-Layer Meteorol.* **147**: 51–82.

Heisenberg W. 1948. On the theory of statistical and isotropic turbulence. *Proc. R. Soc. London A: Math. Phys. Sci.* **195**: 402–406.

Hinze J. 1959. *Turbulence: An Introduction to Its Mechanism and Theory*. McGraw-Hill: New York, NY.

Hsieh CI, Katul GG. 1997. Dissipation methods, Taylor's hypothesis, and stability correction functions in the atmospheric surface layer. *J. Geophys. Res.: Atmos.* **102**: 16391–16405, doi: 10.1029/97JD00200.

Ishihara T, Yoshida K, Kaneda Y. 2002. Anisotropic velocity correlation spectrum at small scales in a homogeneous turbulent shear flow. *Phys. Rev. Lett.* **88**: 154501, doi: 10.1103/PhysRevLett.88.154501.

Kader B, Yaglom A. 1991. Spectra and correlation functions of surface layer atmospheric turbulence in unstable thermal stratification. In *Turbulence and Coherent Structures*, Metais O, Lesieur M. (eds.) 450–467. Kluwer Academic Publishers: Dordrecht, Netherlands.

Kaimal JC. 1973. Turbulence spectra, length scales and structure parameters in the stable surface layer. *Boundary-Layer Meteorol.* **4**: 289–309.

Kaimal J, Finnigan J. 1994. *Atmospheric Boundary-Layer Flows: Their Structure and Measurement*. Oxford University Press: New York, NY.

Kaimal JC, Izumi Y, Wyngaard JC, Cote R. 1972. Spectral characteristics of surface-layer turbulence. *Q. J. R. Meteorol. Soc.* **98**: 563–589.

Katul G, Chu C. 1998. A theoretical and experimental investigation of energy-containing scales in the dynamic sublayer of boundary-layer flows. *Boundary-Layer Meteorol.* **86**: 279–312.

Katul G, Chu C, Parlange M, Albertson J, Ortenburger T. 1995. Low-wavenumber spectral characteristics of velocity and temperature in the atmospheric surface layer. *J. Geophys. Res.* **100**: 14243–14255, doi: 10.1029/94JD02616.

Katul G, Hsieh CI, Sigmon J. 1997. Energy-inertial scale interactions for velocity and temperature in the unstable atmospheric surface layer. *Boundary-Layer Meteorol.* **82**: 49–80.

Katul GG, Porporato A, Nikora V. 2012. Existence of power-law scaling in the equilibrium regions of wall-bounded turbulence explained by Heisenberg's eddy viscosity. *Phys. Rev E* **86**: 066311.

Katul GG, Li D, Chamecki M, Bou-Zeid E. 2013. Mean scalar concentration profile in a sheared and thermally stratified atmospheric surface layer. *Phys. Rev. E* **87**: 023004, doi: 10.1103/PhysRevE.87.023004.

Katul GG, Porporato A, Shah S, Bou-Zeid, E. 2014. Two phenomenological constants explain similarity laws in stably stratified turbulence. *Phys. Rev. E* **89**: 023007, doi: 10.1103/PhysRevE.89.023007.

© 2015 Royal Meteorological Society

Kolmogorov A. 1941. Dissipation of energy under locally isotropic turbulence. *Dokl. Akad. Naukl. SSSR* **32**: 16–18.

Launder B, Reece G, Rodi W. 1975. Progress in the development of a Reynolds-stress turbulence closure. *J. Fluid Mech.* **68**: 537–566.

Li D, Bou-Zeid E. 2011. Coherent structures and the dissimilarity of turbulent transport of momentum and scalars in the unstable atmospheric surface layer. *Boundary-Layer Meteorol.* **140**: 243–262.

Li D, Bou-Zeid E, de Bruin H. 2012. Monin–Obukhov similarity functions for the structure parameters of temperature and humidity. *Boundary-Layer Meteorol.* **145**: 45–67.

Li D, Katul GG, Bou-Zeid E. 2015a. Turbulent energy spectra and cospectra of momentum and heat fluxes in the stable atmospheric surface layer. *Boundary-Layer Meteorol.* **157**: 1–21, doi: 10.1007/s10546-015-0048-2.

Li D, Katul GG, Zilitinkevich S. 2015b. Revisiting the turbulent prandtl number in an idealized atmospheric surface layer. *J. Atmos. Sci.* **72**: 2394–2410.

Lumley J. 1967. Similarity and the turbulent energy spectrum. *Phys. Fluids* **10**: 855–858. doi: 10.1063/1.1762200.

Monin A, Obukhov A. 1954. Basic laws of turbulent mixing in the ground layer of the atmosphere. *Akad. Nauk SSSR Geofiz. Inst. Trudy* **151**: 163–187.

Monin A, Yaglom A. 1971. *Statistical Fluid Mechanics*, Vol. 1. MIT Press: Cambridge, MA.

Obukhov A. 1946. Turbulence in thermally inhomogeneous atmosphere. *Trudy Inta Teoret. Geofiz. Akad. Nauk SSSR* **1**: 95–115.

Panchev S, Syrakov D. 1971. Spectra of thermally stratified turbulent flow with no shear. *Tellus* **23**: 500–505.

Perry AE, Abell CJ. 1975. Scaling laws for pipe-flow turbulence. *J. Fluid Mech.* **67**: 257–271.

Perry AE, Abell CJ. 1977. Asymptotic similarity of turbulence structures in smooth- and rough-walled pipes. *J. Fluid Mech.* **79**: 785–799, doi: 10.1017/S0022112077000457.

Perry A, Henbest S, Chong M. 1986. A theoretical and experimental study of wall turbulence. *J. Fluid Mech.* **165**: 163–199.

Perry A, Marušić I, Li J. 1994. Wall turbulence closure based on classical similarity laws and the attached eddy hypothesis. *Phys. Fluids* **6**: 1024–1035.

Pond S, Smith S, Hamblin P, Burling R. 1966. Spectra of velocity and temperature fluctuations in the atmospheric boundary layer over the sea. *J. Atmos. Sci.* **23**: 376–386.

Pope S. 2000. *Turbulent Flows*. Cambridge University Press: Cambridge, UK.

Schotanus P, Nieuwstadt F, De Bruin H. 1983. Temperature measurement with a sonic anemometer and its application to heat and moisture fluxes. *Boundary-Layer Meteorol.* **26**: 81–93.

Schumann U. 1994. On relations between constants in homogeneous turbulence models and Heisenberg's spectral model. *Inst. Phys. Atmos.* **67**: 141–147.

Sreenivasan K. 1995. On the universality of the Kolmogorov constant. *Phys. Fluids* **7**: 2778–2784.

Sreenivasan K, Antonia R. 1997. The phenomenology of small scale turbulence. *Annu. Rev. Fluid Mech.* **29**: 435–472.

Stull R. 1988. *An Introduction to Boundary-Layer Meteorology*. Kluwer Academic Publishers: Dordrecht, Netherlands.

Sturm P, Eugster W, Knohl A. 2012. Eddy covariance measurements of CO2 isotopologues with a quantum cascade laser absorption spectrometer. *Agric. For. Meteorol.* **152**:73–82.

Sun K, Li D, Tao L, Zhao Z, Zondlo MA. 2015. Quantifying the influence of random errors in turbulence measurements on scalar similarity in the atmospheric surface layer. *Boundary-Layer Meteorol.* **157**: 61–80.

Taylor GI. 1938. The spectrum of turbulence. *Proc. R. Soc. London A* **132**: 476–490.

Tchen CM. 1953. On the spectrum of energy in turbulent shear flow. *J. Res. Nat. Bur. Stand.* **50**: 51–62.

Tchen CM. 1954. Transport processes as foundations of the Heisenberg and Obukhov theories of turbulence. *Phys. Rev.* **93**: 4–14, doi:10.1103/PhysRev.93.4.

Townsend AA. 1976. *The Structure of Turbulent Shear Flow*. Cambridge University Press: Cambridge, MA.

Vercauteren N, Bou-Zeid E, Parlange MB, Lemmin U, Huwald H, Selker J, Meneveau C. 2008. Subgrid-scale dynamics for water vapour, heat and momentum over a lake. *Boundary-Layer Meteorol.* **128**: 205–228.

Wyngaard J, Cote O. 1972. Co-spectral similarity theory in the atmospheric surface layer. *Q. J. R. Meteorol. Soc.* **98**: 590–603.

Zilitinkevich S, Elperin T, Kleeorin N, Rogachevskii I, Esau I. 2013. A hierarchy of energy- and flux-budget (EFB) turbulence closure models for stably stratified geophysical flows. *Boundary-Layer Meteorol.* **146**: 341–373.

© 2015 Royal Meteorological Society